Proceedings of the 40th IAHR World Congress. Rivers – Connecting Mountains and Coasts
21 – 25 August 2023, Vienna, Austria
Edited by Helmut Habersack, Michael Tritthart and Lisa Waldenberger

doi: 10.3850/978-90-833476-1-5_iahr40wc-p0027-cd

Self-aeration in free-surface flows at high Reynolds number (2.6E+6 - 1.1E+8)

Hubert Chanson[(1)]
[(1)] The University of Queensland, School of Civil Engineering, Brisbane QLD 4072, Australia
E-mail: h.chanson@uq.edu.au

Abstract

In self-aerated free-surface flows, the upstream flow is typically non-aerated and the flow becomes a strong air-water mix once the turbulent shear stress acting next to the interface exceeds the combined resistance of capillary effect and gravity. The onset location of air entrapment is a rapidly-varied region with a rapid, sometimes explosive transition from monophase liquid to two-phase gas-liquid flows. In this presentation, field observations were conducted in three large hydraulic structures during major flood events, with corresponding Reynolds numbers ranging from 2.6×10^6 to 1.1×10^8. Visual observations showed that the inception of self-aeration was a complicated three-dimensional transient phenomenon. An optical technique was applied to gain detailed surface velocity data. While the streamwise surface velocities were reasonably close to theoretical considerations, the streamwise surface velocity fluctuations showed large streamwise turbulence in excess of 100%, consistent with self-aerated free-surface flow measurements based upon dual-tip phase detection probes in laboratory. The current findings yields a seminal question: how large the Reynolds number of a prototype flow needs to be truly representative of large dam spillway self-aerated flows?

Keywords: Hydraulic structures, Air entrainment, Prototype observations, Spillway operation, Inception of air entrainment, Surface velocity

1. INTRODUCTION

In self-aerated free-surface high-velocity flows, the upstream flow region is typically non-aerated and a strong air-water mix develops once the turbulent shear stress acting next to the interface exceeds the combined resistance of capillary effect and gravity (Ervine and Falvey 1987, Chanson 2009). At the upstream end of a chute, the flow is rapidly accelerated and a turbulent boundary layer develops along the channel invert. On a steep channel, the inception of self aeration is observed once the turbulence at the outer edge of the developing boundary layer interacts with the free-surface (Hino 1961, Rao and Rajaratnam 1961). The boundary layer-free-surface interactions can be explosive with strong air-water ejections (Chanson 2013,2022, Zabaleta and Bombardelli 2020) (Fig. 1 Top). On flat chutes, the air entrainment onset region presents a rough interface with free-surface instabilities (Michels and Lovely 1953, Chanson 1997) (Fig. 1 Bottom). On these flat-slope chutes, it is thought that the onset of aeration results from a combination of longitudinal vortices' breakdown and of gravity waves produced by roughness and irregularities at the channel boundaries (Levi 1965,1967, Anwar 1994). Yet, the two theories are not exclusive, as recently discussed by Toro et al. (2017) and Chanson (2022). Typical self-aeration processes are illustrated in Figure 1, with a series of high-shutter speed photographs of prototype chute operations.

The following paper aims to discuss the self-aeration inception process in prototype hydraulic structures operating with Reynolds numbers between 2.6×10^6 and 1.1×10^8. The prototype observations were undertaken during major flood events between 2010 and 2022 in eastern Australia. Some key features of the onset of self-aeration are described. Detailed observations of the surface velocity fields are presented, showing that the self-aerated gas-liquid flow is characterised by large streamwise surface velocity fluctuations.

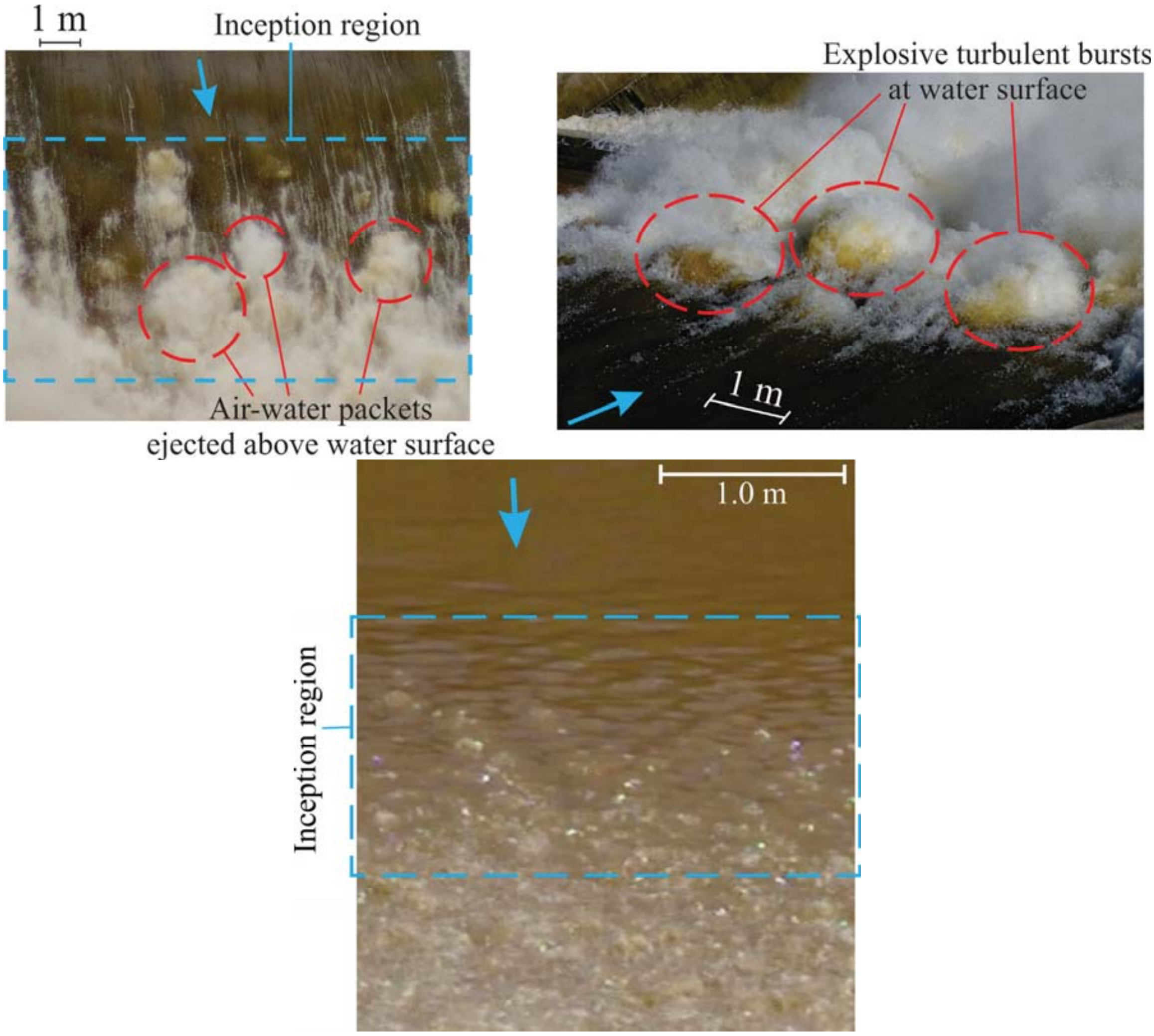

Figure 1. High-shutter speed photographs of self-aerated free-surface flows on prototype spillways. Top: steep staircase chute, Hinze dam, March 2022, Re = 3.6×10^7 (Left) and 2.8×10^7(Right); Bottom: flat smooth chute, Chinchilla weir, December 2021 (Re = 2.7×10^6 to 4.6×10^6).

2. PHYSICAL MEASUREMENTS AT PROTOTYPE SPILLWAYS

Prototype observations were conducted at three dam spillways between 2010 and 2022. These are the Paradise Dam stepped spillway in 2010 and 2013, the Hinze Dam stepped spillway between 2013 and 2022, and the Chinchilla Weir in 2021 (Table 1). In Table 1, the flow conditions during the observations are summarised with the Reynolds number Re being defined in terms of the equivalent pipe diameter. All these hydraulic structures are listed as "Large Dam" by the Australian committee on large dams (ANCOLD) and the international committee on large dams (ICOLD).

The Paradise dam is a roller compacted concrete (RCC) structure equipped with a 315 m wide primary stepped spillway and an un-controlled ogee crest. The final chute slope is 1V:0.64H (57.38°) with 0.62 m high steps. Photographic observations were conducted from the right bank of the stilling basin (Fig. 2 Top).

The Hinze dam spillway is a steep stepped chute, followed by an energy dissipator located about 35 m below the chute crest. The final chute slope is θ = 51.3° and the steps are 1.5 m high (Fig. 2 Middle). The low section is 12.25 m wide. Photographic and cinematographic observations were undertaken from reinforced concrete platforms, one located downstream of and facing the chute, and a second one above the chute crest centreline (Chanson 2022).

The Chinchilla weir is a 14 m high earthfill embankment, with an overflow spillway channel. The chute consists of a broad crest, followed by a 60.6 m long smooth converging channel with a slope θ = 11.3° (Fig. 2 Bottom). The chute convergence is $\partial B/\partial x$ = -2.18 m/m. The overflow channel is made of concrete slabs, with a series of drains to reduce seepage pressure (Turnbull and McKay 1974). Observations were conducted from the right bank and from downstream, facing the left spillway bay (Chanson and Apelt 2022,2023).

Visual, photographic and cinematographic data were collected during a number of major flood events (Table 1). The observations were documented using dSLR cameras Pentax™ K-7, K-01 and K-3 with sensor resolutions between 12 Mpx and 24 Mpx, complemented by digital cameras Casio™ EX10 Exilim and Sony™ RC100VA, and an iPhone XI. The dSLR cameras were equipped with full-frame prime lenses producing photographs and movies with negligible barrel distortion and two zoom lenses. The latters were used primarily for qualitative and limited quantitative observations. The dSLR camera movies were recorded in high definition (1920×1080 px) at 30 fps and 60 fps.

The analyses of air-water surface features were performed based upon high-shutter speed photographs and cinematographic movies. Herein, all the tracking and measurements of air-water features were undertaken manually to ensure the best quality control, because of the complexity of the prototype turbulent motion, which was characterised by extremely rapid and pseudo-random changes with space and time. In addition, a number of movies, collected with dSLR cameras equipped with full-frame prime lenses, were processed using an optical flow (OF) technique, with the camera fixed on a sturdy tripod. The OF is a set of tools, detecting the flow motion between consecutive frames based upon brightness intensity changes, originally developed by computer vision scientists (Bung and Valero 2016, Zhang and Chanson 2019). Herein, the OF technique was based the Farneback method. The Farneback technique was applied using parameters previously obtained and validated in laboratory for surface velocity (Arosquipa Nina et al. 2022). The application to prototype spillway chutes was carefully validated against theoretical analyses and large-size physical model (Chanson 2022, Chanson and Apelt 2022).

Table 1. Prototype observations in eastern Australia (Current study).

Spillway	Design	θ (°)	Date	Q (m^3/s)	q (m^2/s)	Re	Comment
Paradise dam	Stepped	57.4	30/12/2010	5,965	18.9	7.5×10^7	
			5/03/2013	2,316	7.4	2.9×10^7	
Hinze dam	Stepped	51.3	29/01/2013	202	16.5	6.5×10^7	Also Chanson (2013)
			3/05/2015	21	1.7	6.8×10^6	
			31/03/2017	224	27.3	1.1×10^8	1:100 AEP flood
			23/03/2021	111	9.1	3.6×10^7	
			24/03/2021	140	11.4	4.5×10^7	
			27/03/2021	72	5.9	2.3×10^7	
			25/02/2022	52	4.3	1.7×10^7	
			27/02/2022	116	9.5	3.8×10^7	
			1/03/2022	249	20.4	8.1×10^7	
			3/03/2022	143	11.7	4.6×10^7	
			4/03/2022	111	9.1	3.6×10^7	
			5/03/2022	86	7.0	2.8×10^7	
Chinchilla weir	Smooth	11.3	27/11/2021	121	0.57 / 1.0	2.3×10^6 / 4.6×10^6	
			15/12/2021	144	0.67 / 1.16	2.7×10^6 / 4.6×10^6	

Figure 2. Self-aeration at prototype spillways during major flood operation. Top: Paradise Dam spillway for Re = 2.9×10^7 (Left) and 7.5×10^7 (Right). Middle: Hinze Dam spillway for Re = 6.5×10^7 (Left) and 8.1×10^7 (Right). Bottom: Chinchilla weir for Re = 2.7×10^6 / 4.6×10^6. All photographs are high shutter speed with exposure time < 1 ms.

3. PROTOTYPE OBSERVATIONS

During all the flood events, the approach flow to the chute was observed to very smooth at all hydraulic structures, as confirmed by aerial photographs and drone footages during a select number of events (Fig. 3). The inflow converged smoothly towards the chute crest and the upstream water surface was waveless and almost still. On all occasions, the flow was critical at the un-controlled crest which acted as a hydraulic control. The smooth change on water surface elevation between the upstream reservoir and the upstream end of the chute was nicely documented with photographs and movies.

As the flow accelerated down the chute, the free-surface become rough and choppy, before becoming self-aerated. The inception region presented marked difference between flat-slope and steep slope structures. At flat-slope structures, a progressive transition of surface roughness was seen, as documented at Chinchilla weir in 1997, 2011, 2021 and 2022 (Chanson and Apelt 2023), as well as at other flat-slope chute structures (Anwar 1994). Down un-controlled flat-slope chutes, the water surface changes progressively from a glassy surface to a rough appearance, followed by a choppy wavy texture, becoming self-aerated, i.e. the inception region (Fig.1 Bottom). The inception region corresponded to the progressive change in surface roughness and texture. Downstream of the inception region, the self-aerated chute flow at Chinchilla weir consistently exhibited a beige colour, as documented in 1974, 1997, 2011, 2021 and 222, which was caused by the three-phase nature of the air-water sediment motion.

At steep slope chutes, in contrast, the inception region was characterised by explosive interactions between large-scale turbulent structures and the water surface (Figs. 1 Top, 2 Top and Middle, & 4A). Short-lived very-energetic surface boils and scars were seen immediately upstream of the inception of free-surface aeration. Visually, the surface scars initiated and developed primarily as transverse entities, although the generation process could include a mix of both longitudinal and transverse scar initiation (Chanson 2022). Figure 4B presents the dimensionless growth of the transverse width of air-water surface features in the vicinity of the onset region. The data include both prototype and laboratory observations obtained with high-shutter speed records (Table 2). In Table 2, the aspect ratio B/d_c is included and defined as the ratio of chute width B to critical depth flow d_c. For the data sets (Table 2), the growth of transverse cars was best correlated by (Fig. 4B)

$$\frac{w}{d_c} = 0.888 \times \left(t \times \sqrt{\frac{g}{d_c}} \right)^{0.485} \qquad \text{Steep-slope chutes [1]}$$

with w the instantaneous width, g the gravity acceleration, t the time since the apparition of the surface feature, and a normalised correlation coefficient of 0.80. Equation [1] is compared to both prototype and laboratory data in Figure 4B.

The scar features were linked to some violent upwelling of large-scale elongated coherent structures. As the surface breaking took place, some upward stretching of the scar occurred, with violent air-water processes including air-water fluid expulsion and air entrapment. While the upwelling continued, the violent surface breaking led to the formation of elongated air-water surface features (Fig. 4A). Ultimately, the growth of the elongated air-water surface features lead to the complete aeration of the whole free-surface, i.e. the "white waters" downstream of the inception region. Intringingly, the air-water surface features were elongated in prototype chutes with length to width ratios typically greater than 2 to 5, e.g. at Hinze and Paradise Dams (Present study), at Pedrogao Dam (Matos and Meireles 2014), and at Aviemore Dam (Keller 1972, Cain 1978). In contrast, the air-water surface features in laboratory presented an aspect ratio equal to unity in average (Fig. 4C). The contrasting observations between prototype and laboratory data hint that laboratory investigations of self-aerated flows might not be extrapolated to prototype applications without some intrinsic limitations including potential scale effects, already mentioned elsewhere (Wood 1985, Chanson 1995, Zhang and Chanson 2017).

Figure 3. Approach flow conditions at Paradise Dam and Chinchilla weir during major flood operations. Left: Paradise Dam on 30 December 2010 for Re = 7.5×10^5; Right: Chinchilla weir on 6 April 2022 for Re ~ 6×10^6 (Photo NearMap).

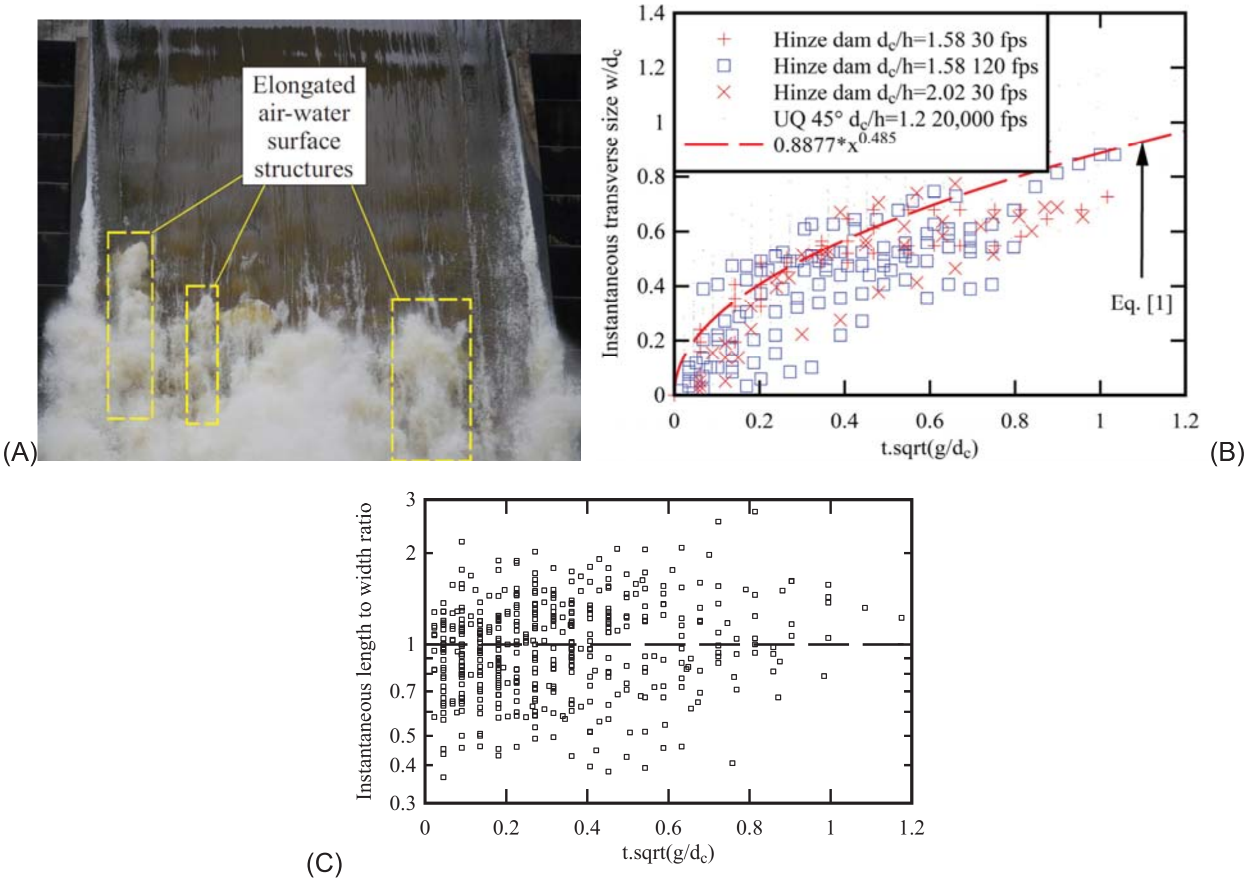

Figure 4. Inception region in steep-slope chute. (A) Elongated air-water surface features in the vicinity of the inception region Hinze Dam spillway for Re = 3.6×10^7 (shutter speed: 1/1,000 s); (B) Dimensionless transverse growth of individual surface scars in prototype and laboratory (Table 2); (C) Dimensionless time-variations of length to width ratio of individual surface scars in laboratory (Table 2)

Table 2. Quantitative observations of individual air-water surface features in the inception region of steep-slope prototype and laboratory spillway chutes (Current study).

Spillway	Design	θ (°)	Q (m^3/s)	q (m^2/s)	Re	Aspect ratio B/d_c	Camera frame rate
Hinze dam	Stepped (h=1.5 m)	51.3	140	11.4	4.5×10^7	5.16	30 fps
			140	11.4	4.5×10^7	5.16	120 fps
			202	16.5	6.5×10^7	4.04	30 fps
Laboratory (UQ)	Stepped (h=0.10 m)	45.0	0.13	0.13	5.2×10^5	8.21	20,000 fps

The mean location of the inception region of self-aeration was recorded during all overflows, and the data are presented in Figure 5A, as L_I/d_c as function of the Reynolds number. Despite differences in designs, such as smooth versus stepped chutes and flat versus steep slopes, the prototype data were reasonably well correlated by:

$$\frac{L_I}{d_c} = 9 + \frac{4.65\times10^5}{Re^{0.7}} \quad [2]$$

with L_I the mean position of inception region of free-surface aeration measured from the chute crest and a normalised correlation coefficient of 0.96. Equation [2] is compared to the prototype data in Figure 2, showing an upper limit L_I/d_c towards 9 for very large Reynolds numbers, irrespective of the invert type and chute slope.

The dimensionless depth data d_I/d_c in the inception region are presented in Figure 5B. Despite some scatter, the prototype data showed smaller water depths at inception on smooth chutes, compared to stepped chutes. While differences are seen among stepped chute data, it is important to stress the high accuracy of the Hinze Dam data set, thanks to the excellent and unique physical and optical access (Chanson 2022).

The OF surface velocity data showed a longitudinal distribution with increasing surface velocity V_s with decreasing vertical invert elevation z_o at both Hinze Dam and Chinchilla weir (Chanson 2022, Chanson and Apelt 2023) (Fig. 6 Top). At both structures, the longitudinal surface velocity data showed "canyons" of higher velocities, which invalidated the "traditional" design assumption of one-dimensional flow on spillway chutes. The standard deviations of streamwise and transverse surface velocity showed large streamwise surface turbulence and much smaller transverse turbulent intensity. The dimensionless longitudinal velocity fluctuations v_s'/V_s were of the order of magnitude of unity: $v_s'/V_s \propto 1$ at both structures (Fig. 6 Bottom). The data were close to laboratory observations of surface velocity fluctuations of Arosquipa Nina et al. (2022). This is shown in Figure 6 (Bottom Right), comparing prototype observations with laboratory observations using optical (OF) technique and based upon interfacial turbulence data using dual-tip phase detection probe (DTPDP). Altogether, the prototype surface velocity and turbulence contour maps demonstrated a strong three-dimensionality of the prototype self-aerated chute flows with direct implications into in the design of downstream stilling basins.

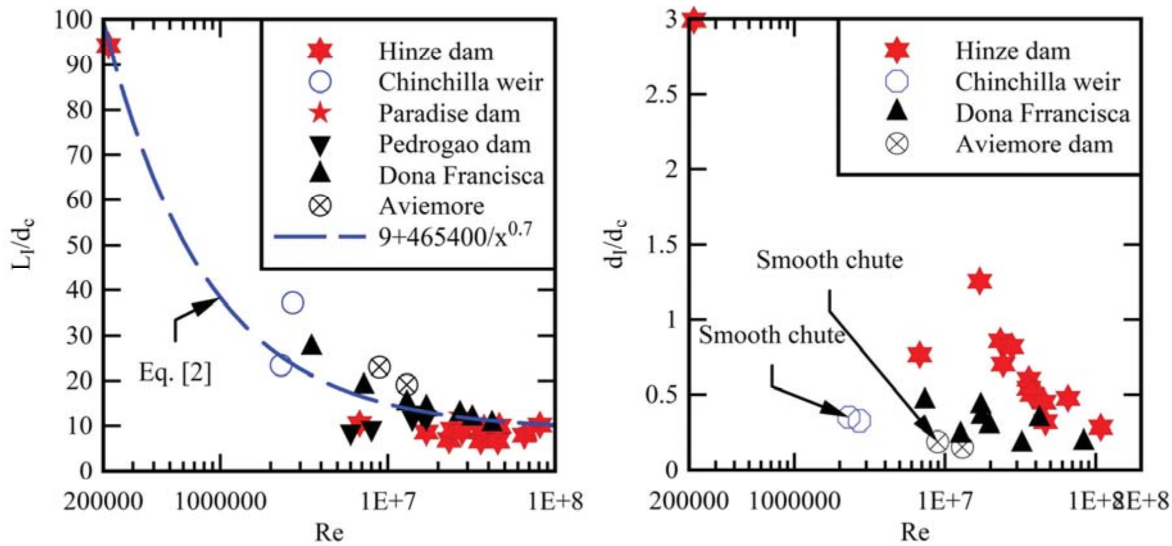

Figure 5. Dimensionless location L_I of and water depth d_I of the inception region in prototype spillway chutes. Left: longitudinal location of the inception region incl. comparison with Eq. [2]; Right: water depth in the inception region. Comparison between prototype smooth chute data (Aviemore dam, Chinchilla weir) and prototype stepped chute data (Hinze dam, Paradise dam, Pedrogao dam, Dona Francisca dam).

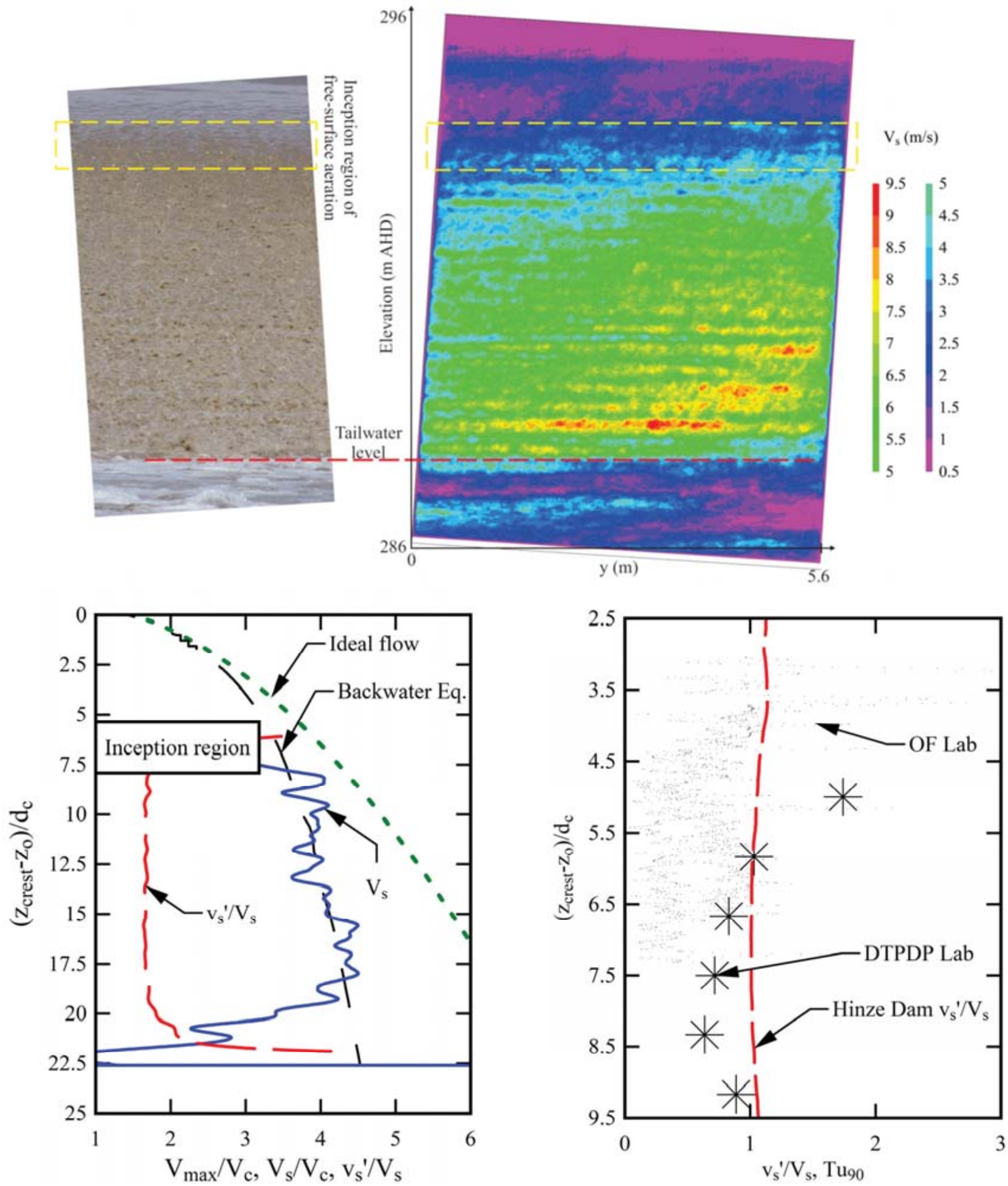

Figure 6. Surface velocity measurements at prototype spillways during major flood operation. Top: Magnitude of longitudinal surface velocity V_s at Chinchilla weir's left spillway bay for Re = 2.3×10^6 / 4.6×10^6. Bottom: vertical variation of time-averaged longitudinal velocity V_s and turbulence intensity v_s'/V_s at Chinchilla weir for Re = 2.7×10^6 / 4.6×10^6 (Left); vertical variation of turbulence intensity v_s'/V_s at Hinze Dam for Re = 4.5×10^7 and at the University of Queensland for Re = 5.2×10^5 (Right). Note that the critical flow conditions (d_c, V_c) are calculated at the spillway crest.

4. DISCUSSION AND CONCLUDING REMARKS

In a world experiencing hydrological and hydraulic extremes with droughts and floods, the society needs both water security and flood protection (Jonkman 2005, Rojas et al. 2013). Dams and reservoirs constitute the most efficient means to deliver both (Novak et al. 2007). Dams must be equipped with a spillway system to pass safely the flood waters above, below, beneath or beside the dam wall. But *what do we know really about prototype spillway operation, beyond visual qualitative observations and physical modelling in small size facilities*? Detailed observations of prototype spillway overflow are rare, especially during large floods. The prototype field measurements are uppermost important because they apply to the full-scale infrastructure. Despite a number of intrinsic difficulties, they represent the ultimate data set. In plain terms, quantitative prototype data constitute a fundamental requirement for the proper validation of successful hydraulic designs and of both experimental and computational modelling. While it is acknowledged that many variables are uncontrolled during prototype hydraulic structure overflows, recent developments in physical and optical observations delivered a few prototype data sets (Cain and Wood 1981, Volkart and Rutschmann 1984, Bai et al. 2022, Chanson 2022, Chanson and Apelt 2023).

Yet, an expert hydraulic engineer should ask: **how large the Reynolds number of a prototype flow needs to be?** Let us remember that the flow conditions at the Aviemore dam spillway (Cain and Wood 1981), La Grande Dixence spillway chute (Volkart and Rutschmann 1984), Pangzhuang gate (Bai et al. 2021) and Chinchilla weir (Chanson and Apelt 2023) corresponded to Reynolds numbers Re about 10^6 to 3×10^6, i.e. one to two orders of magnitude lower than the design flow conditions of many large spillway systems including the Hinze Dam and Paradise Dam spillway chutes. The present contribution encompasses prototype data collected at large Reynolds numbers up to 1.1×10^8, and constitutes an unique and seminal attempt to expand the state-of-the art expertise in air-water flows in free-surface flow.

5. ACKNOWLEDGEMENTS

The author thanks many people for their assistance during the field observations (Ms Ya-Hui Chou, André Chanson, Bernard Chanson) and data processing (Dr Rui Shi, Prof. Colin J. Apelt, Barton Maher, Leigh Cook and Tobias Burwood) as well as several agencies (Seqwater, Sunwater, Western Downs Regional Council). He also acknowledges data provided by Prof. Jorge Matos and Mr Rui Yang.

6. REFERENCES

Anwar, H.O. (1994). "Self-Aerated Flows on Chutes and Spillways - Discussion." *Journal of Hydraulic Engineering*, ASCE, Vol. 120, No. 6, pp. 778-779.

Arosqyuipa Nina, Y, Shi, R., Wüthrich, D., and Chanson, H. (2022). "Intrusive and Non-Intrusive Two-Phase Air-Water Measurements on Stepped Spillways: a Physical Study." *Experimental Thermal and Fluid Science*, Vol. 131, Paper 110545, 22 pages, 4 movies and a digital appendix (6 pages) (DOI: 10.1016/j.expthermflusci.2021.110545).

Bai, Z., Bai, R., Tang, R., Wang, H., and Liu, S. (2021). "Case Study of Prototype Hydraulic Jump on Slope: Air Entrainment and Free-Surface Measurement." Journal of Hydraulic Engineering, ASCE, Vol. 147, No. 9, Paper 05021007, 12 pages (DOI: 10.1061/(ASCE)HY.1943-7900.0001916).

Bung, D.B., and Valera, D. (2016). "Optical Flow Estimation in Aerated Flows." *Journal of Hydraulic Research*, IAHR, Vol. 54, No. 5, pp. 575-580 (DOI: 10.1080/00221686.2016.1173600).

Cain, P. (1978). "Measurements within Self-Aerated Flow on a Large Spillway." *Ph.D. Thesis*, Ref. 78-18, Dept. of Civil Engrg., Univ. of Canterbury, Christchurch, New Zealand.

Cain, P., and Wood, I.R. (1981). "Measurements of Self-aerated Flow on a Spillway." *Jl. Hyd. Div.*, ASCE, 107, HY11, pp. 1425-1444.

Chanson, H. (1995). "Air Bubble Diffusion in Supercritical Open Channel Flow." *Proc. 12th Australasian Fluid Mechanics Conference AFMC*, Sydney, Australia, R.W. Bilger Editor, Vol. 2, pp. 707-710

Chanson, H. (1997). "Air Bubble Entrainment in Open Channels. Flow Structure and Bubble Size Distributions." *International Journal of Multiphase Flow*, Vol. 23, No. 1, pp. 193-203 (DOI: 10.1016/S0301-9322(96)00063-8)

Chanson, H. (2009). "Turbulent Air-water Flows in Hydraulic Structures: Dynamic Similarity and Scale Effects." *Environmental Fluid Mechanics*, 9(2), 125-142 (DOI: 10.1007/s10652-008-9078-3).

Chanson, H. (2013). "Interactions between a Developing Boundary Layer and the Free-Surface on a Stepped Spillway: Hinze Dam Spillway Operation in January 2013." *Proc. 8th International Conference on Multiphase Flow ICMF 2013*, Jeju, Korea, 26-31 May, Gallery Session ICMF2013-005 (Video duration: 2:15) {https://espace.library.uq.edu.au/view/UQ:301643}.

Chanson, H. (2022). "Stepped Spillway Prototype Operation and Air Entrainment: Toward a Better Understanding of the Mechanisms Leading to Air Entrainment in Skimming Flows." *Journal of Hydraulic Engineering*, ASCE, Vol. 148, No. 11, Paper 05022004, 17 pages (DOI: 10.1061/(ASCE)HY.1943-7900.0002015).

Chanson, H., and Apelt, C.J. (2022). "Surface Velocities and Free-surface Aeration in a Converging Smooth Chute during a Major Flood Event." *Proceedings of the 9th IAHR International Symposium on Hydraulic Structures ISHS2022*, 24-27 October 2022, Roorkee, India, M. Palermo, Z. Ahmad, B. Crookston and S. Erpicum Editors, Utah State University, Logan, USA, pp. 180-189 (DOI: 10.26077/11eb-458d).

Chanson, H., and Apelt, C.J. (2023). "Environmental Fluid Mechanics of Minimum Energy Loss Weirs: Hydrodynamics and Self-aeration at Chinchilla MEL Weir during the November-December 2021 Flood Event." *Environmental Fluid Mechanics*, 25 pages, DOI: 10.1007/s10652-023-09926-0 (Onine First).

Ervine, D.A., and Falvey, H.T. (1987). "Behaviour of Turbulent Water Jets in the Atmosphere and in Plunge Pools." *Proceedings of the Institution Civil Engineers, London*, Part 2, 83, 295-314.

Hino, M. (1961). "A Theory of the Mechanism of Self-Aerated Flow on Steep Slope Channels. Applications of the Statistical Theory of Turbulence." *Technical Report C-6101*, Technical Laboratory, Central Research Institute of Electric Power Industry, Japan, 42 pages.

Jonkman, S.N. (2005). "Global perspectives on loss of human life caused by floods." *Natural Hazards*, Vol. 34, pp.151–175.

Keller, R.J. (1972). "Field Measurement of Self-Aerated High Speed Open Channel Flow." *Ph.D. thesis*, Dept. of Civil Eng., Univ. of Canterbury, New Zealand.

Matos, J., and Meirales, I. (2014). "Hydraulics of stepped weirs and dam spillways: engineering challenges, labyrinths of research." *Proceedings of the 5th IAHR International Symposium on Hydraulic Structures (ISHS2014)*, 25-27 June 2014, The University of Queensland, Brisbane, Australia, H. Chanson and L. Toombes Editors, 30 pages (DOI: 10.14264/uql.2014.11).

Levi, E. (1965). "Longitudinal Streaking in Liquid Currents." *Journal of Hydraulic Research*, IAHR, Vol. 3, No. 2, pp. 25-39.

Levi, E. (1967). "Macroturbulence Produced by Vortex Breakdown in High Velocity Flows." *Proc. 12th IAHR Congress*, Colorado, USA, Vol. 2, Paper B7, pp. 54-60.

Michels, V., and Lovely, M. (1953). "Some Prototype Observations of Air Entrained Flow." *Proc. 5th IAHR Congress*, IAHR-ASCE, Minneapolis, USA, pp. 403-414.

Novak, P., Moffat, A.I.B., Nalluri, C., and Narayanan, R. (2007). "Hydraulic Structures." *Taylor & Francis*, London, UK, 4th edition, 700 pages.

Rao, N.S.G., and Rajaratnam, N. (1961). "On the Inception of Air Entrainment in Open Channel Flows." *Proc. 9th IAHR Congress*, Dubrovnick, Yugoslavia, pp. 9-12.

Rojas, R., Feyen, L., and Watkiss, P. (2013). "Climate change and river floods in the European Union: socio-economic consequences and the costs and benefits of adaptation." *Glob Environ Change*, Vol. 23, pp. 1737-1751

Toro, J.P., Bombardelli, F.A., and Paik, J. (2017). "Detached Eddy Simulation of the Nonaerated Skimming Flow over a Stepped Spillway." *Journal of Hydraulic Engineering*, ASCE, Vol. 143, No. 9, Paper 04017032, 14 pages.

Turnbull, J.D., and McKay, G.R. (1974). "The Design and Construction of Chinchilla Weir - Condamine River Queensland." *Proc. 5th Australasian Conference on Hydraulics and Fluid Mechanics*, Christchurch, New Zealand, Vol. II, pp. 1-8.

Volkart, P., and Rutschmann, P. (1984). "Rapid Flow in Spillway Chutes with and without Deflectors - A Model-Prototype Comparison." *Proc. Intl. Symp. on Scale Effects in Modelling Hydraulic Structures*, IAHR, Esslingen, Germany, H. KOBUS editor, paper 4.5.

Wood, I.R. (1985). "Air Water Flows." *Proc. 21st IAHR Congress*, Melbourne, Australia, Keynote address, pp. 18-29.

Zabaleta, F., and Bombardelli, F.A. (2020). "Eddy-resolving Simulation of Flows over Macroroughness." *Proceedings of RiverFlow2020*, CRC Press, Uijttewaal et al. Editors, pp. 1293-1299.

Zhang, G., and Chanson, H. (2017). "Self-aeration in the rapidly- and gradually-varying flow regions of steep smooth and stepped spillways." *Environmental Fluid Mechanics*, Vol. 17, No. 1, pp. 27-46 (DOI: 10.1007/s10652-015-9442-z)

Zhang, G., and Chanson, H. (2019). "Application of Optical Flow Methods to Aerated Skimming Flows above Triangular and Trapezoidal Step Cavities." *Journal of Hydraulic Research*, IAHR, Vol. Vol. 57, No. 4 (2019), pp. 488-497 (DOI: 10.1080/00221686.2018.1489900)